접착 및 계면 제21권 제1호, 2020년
〈연구논문(Original Article)〉

Journal of Adhesion and Interface Vol.21, No.1, 2020
https://doi.org/10.17702/jai.2020.21.1.20

Shear Strength of an Aluminum Alloy Bonded with a DP-460 Adhesive: Single Lap-shear Joints

Hyun-Bum Kim[1†] · Tomohisa Nishida[1] · Hiroyuki Oguma[2] · Kimiyoshi Naito[2]

[1]*Mechanical Engineering, National Institute of Technology, Numazu College, 3600 Ooka, Numazu City, Shizuoka 410-8501, Japan*
[2]*National Institute for Materials Science, Bonding and Manufacturing Field, Polymer Matrix Hybrid Composite Materials Group, Research Center for Structural Materials, 1-2-1 Sengen, Tsukuba, Ibaraki 305-0047, Japan*

(Received December 26, 2019, Revised January 28, 2020; Accepted February 13, 2020)

Abstract: Single lap-shear joints (SLJ) specimens with and without partial round fillets were fabricated to measure the average shear strength of adhesives. The effects of the length of the adherend on the SLJ specimens were also investigated. An epoxy adhesive was used to bond aluminum alloy. Tensile tests were performed on the adhesive bulk specimens to measure the mechanical properties. The finite element analysis (FEA) method was used to measure the adhesive stress distributions, i.e., the peel and shear stresses, on the bonded part. The experimental results revealed that the specimen consisting short length of adherend and without the partial round fillets exhibited the smallest average shear strength of adhesive among the investigated specimens. FEA revealed that the low average shear strength for the specimen with a short adherend length was caused by high stress concentrations on the adhesive at the edge of the bonded part.

Keywords: *Adhesives, Aluminum alloy, Finite element analysis, Stress concentration*

1. Introduction

Adhesives were adopted as structural fastening techniques [1]. Knowing the strength of adhesives on bonded joints with different geometries and loadings and composed of materials with different properties is important [2]. The strength of an adhesive bond-line depends on several factors, including the adhesive type and cure cycle, adherend type and pretreatment, and bond-line thickness [3]. It was reported that bonded joints can be divided into four basic types: single lap, double lap, scarf, and stepped lap [4]. Single lap-shear joints (SLJ) have been used to measure the shear strength of adhesives because of the simple corresponding experimental method [5].

Composite materials have been used as structural materials in joint systems because of their advantages of being lightweight and highly corrosion resistant [6-9]. Carbon/epoxy laminates bonded with an epoxy adhesive for SLJ specimens were studied with different overlap lengths and corner geometries (square and spew fillets) under static and fatigue loadings [10]. The specimens having the spew fillets showed higher shear and fatigue strengths than those of square edges in static and fatigue tests. The adhesive bonding of unidirectional carbon-epoxy with epoxy adhesives were studied to estimate the influence of the cohesive zone model using the SLJ specimens [11]. High-strength steel bonded to three different adhesives was studied to investigate the effect of the adhesive thickness using SLJ specimen [12]. Results showed that the different lap shear strengths were attributed to the stresses between the adhesive-adherend interfaces.

Aluminum alloy has also been used in the automotive and aerospace industries. SLJ specimens of aluminum alloy bonded with an epoxy adhesive have been investigated [13,14]. The edges of the bonded part in SLJ specimens with and without spew fillets were also studied [15]. The results revealed that the specimens with the spew fillets showed less adhesive stress distribution than specimens without the spew fillets at the edge of the bonded part. However, the experimental data for the shear strength of adhesives were not sufficiently investigated in

† Corresponding author: Hyun-Bum Kim (hyunbum.kim@numazu-ct.ac.jp)

terms of the relation between the length of the adherend and corner geometry.

The aim of the present study is to measure the average shear strength on SLJ joints bonded with an epoxy adhesive with different lengths of adherends. SLJ specimens with and without partial round fillets were also investigated. Tensile tests on adhesive bulk specimens were conducted to determine their mechanical properties, e.g., tensile strength and Young's modulus. Finite element analysis (FEA) methods were used to evaluate the adhesive stress distributions, i.e., peel and shear stresses. Fracture surfaces of the SLJ specimens were observed using a microscope.

2. Experimental Procedures

2.1. Materials

Aluminum alloy 5052-H34 (average thickness = 3.0 mm) was used as adherends. A two-part epoxy adhesive (3M™ Scotch-Weld™ epoxy adhesive DP460 off-white, Japan) was used to bond the adherends. The advantages of this adhesive include a high peel strength, high shear strengths, high durability, and easy mixing [16].

2.2. Specimen preparation

2.2.1. Adhesive bulk specimens

The shape and dimensions of the adhesive bulk specimens for the tensile tests are shown in Fig. 1 [17] Dog-bone-shaped tensile test specimens were prepared according to standard JIS K 6251 (No. 6 dumbbell) [18] Silicone rubber with a thickness of 3 mm was punched out to form a dog-bone-shaped mold into which the adhesive was poured. The dog-bone-shaped tensile testing specimens were removed from the mold after curing for 24 h. The surfaces of the adhesive specimens were polished with sandpaper and a liquid diamond compound.

2.2.2. SLJ Specimens

Fig. 2 shows the shape and dimensions of the SLJ specimens manufactured according to standard JIS S 6040 [19]. The SLJ specimens were manufactured at room temperature using toggle clamps and were cured for 24 h. The surfaces of the overlap were sandblasted and subsequently cleaned with acetone. The SLJ specimens without and with a partial round fillet were also fabricated, as shown in Fig. 3 (a) and (b), respectively. The names subsequently assigned to the SLJ specimens

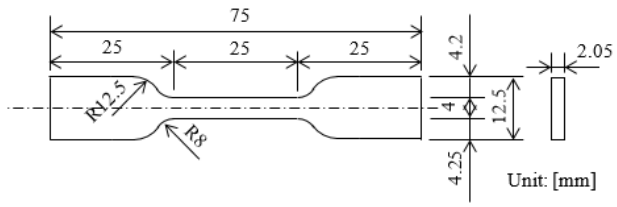

Figure 1. Shape and dimensions of an adhesive bulk specimen for tensile tests[14].

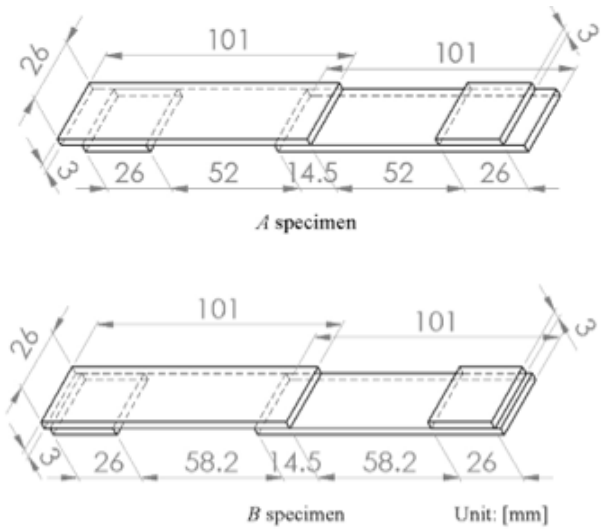

Figure 2. Shape and dimensions of the single lap-shear joint (SLJ) specimens for tensile tests.

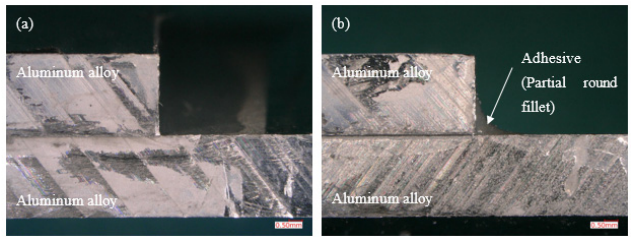

Figure 3. Side views of the single lap-joint (SLJ) specimens; (a) and (b) are the SLJ specimens with and without partial round fillets, respectively.

are listed in Table 1. Four specimens corresponding to each condition were prepared. The bond-line thickness was measured using a micrometer (0.001 mm, MDC-25MJ, Mitutoyo Corporation, Japan). The average bond-line thicknesses for the A, A_r, B, and B_r specimens were 3.42, 12.11, 16.17, and 11.17 μm, respectively. The average radii of the partial round fillets for the A_r and B_r specimens were 2.16 and 2.44 mm, respectively.

Table 1. Assigned names of single lap-shear joint specimens

	Specimens			
	A	A_r	B	B_r
Partial round fillets	×	○	×	○

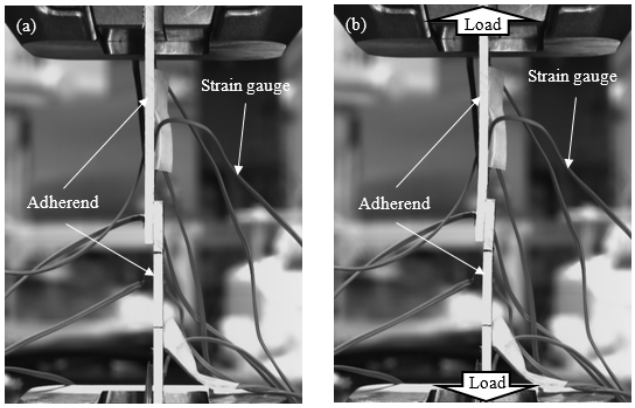

Figure 4. Experimental setup (side views) of single lap-shear joints specimens for the tensile tests; photos (a) and (b) were taken before and during the tensile tests, respectively.

2.3. Tensile tests

Tensile tests for the adhesive bulk specimens were conducted using a tensile test machine (compact table-top universal/tensile tester, EZ-S, Shimadzu Corp., Japan) at a crosshead speed of 1 mm/min. The average cross-sectional area was measured at three locations using a micrometer. Strain was measured using a strain gauge (gauge length of 1 and 5 mm, Kyowa Electronic Instruments Co., Ltd., Japan) attached to both sides of the surface during each test and using a noncontact video extensometer (DVE-201, Shimadzu Corp., Japan) [17]. The Young's modulus (linear portion of strain between 0.2% and 0.4%) was determined from the stress-strain curves recorded using a strain gauge. Nine specimens were measured, and their average value was calculated.

3. Results and Discussion

Tensile tests for the SLJ joint specimens were conducted using a tensile test machine (AG-X, 50 kN floor model, Shimadzu Corp., Japan) at a crosshead speed of 1 mm/min at room temperature. Fig. 4(a) shows the experimental setup of an SLJ joint specimen before loading. The upper and lower adherends are aligned straight in the vertical direction. However, the upper and lower adherends were symmetrically bent as the load was applied to the SLJ specimens, as shown in Fig. 4(b).

Table 2. Mechanical properties of the bulk adhesive specimens. The Young's modulus and Poisson's ratio were measured from the stress-strain curves. Fracture strain was obtained using a noncontact video extensometer

	Tensile strength	Young's modulus (strain gauge)	Young's modulus (noncontact video extensometer)	Poisson's ratio	Fracture strain (noncontact video extensometer)
Average	40.44 [MPa]	2.38 [GPa]	2.24 [GPa]	0.37	6.68 [%]
C.V. [%]	5.68	5.10	5.71	3.17	18.75

(C.V. indicates coefficient of variation.)

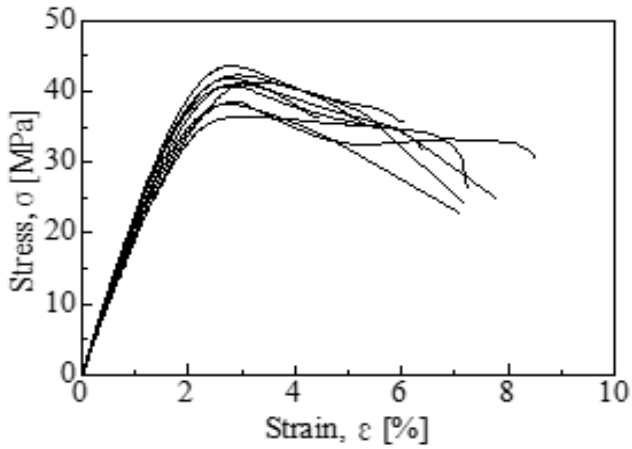

Figure 5. Stress-strain curves for the adhesive bulk specimens. The values of strain were measured using a noncontact video extensometer.

3.1. Stress-strain curves for adhesive bulk specimens

Fig. 5 shows the stress-strain curves for the bulk adhesive specimens, as recorded using a noncontact video extensometer. Table 2 lists the mechanical properties of the bulk adhesive specimens. The fracture strain was measured with a noncontact video extensometer. The average values of tensile strength, Poisson's ratio, and fracture strain were 40.44 MPa, 0.37, and 6.68%, respectively. The Young's moduli measured by strain gauges and a noncontact video extensometer were 2.38 and 2.24 GPa, respectively. The coefficient of variation (C.V.) values for the tensile strength, Young's modulus, and the Poisson's ratio were less than 10%. These results indicate that little variation was observed among the bulk adhesive specimens.

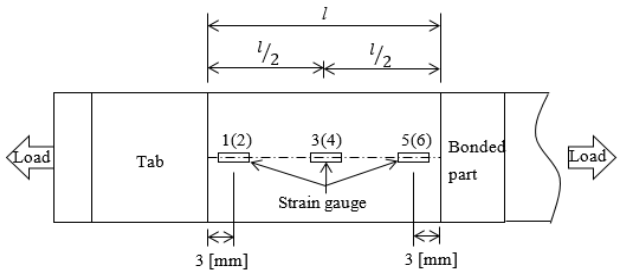

Figure 6. Schematic of single lap-shear joint specimens. Numbers 1, 3, and 5 are the strain gauges attached to the front side of the adhered. The numbers in parentheses (2, 4, and 6) are the strain gauges attached to the backside of the adherend. Strain gauges were attached symmetrically to an SLJ specimen (see Fig. 4).

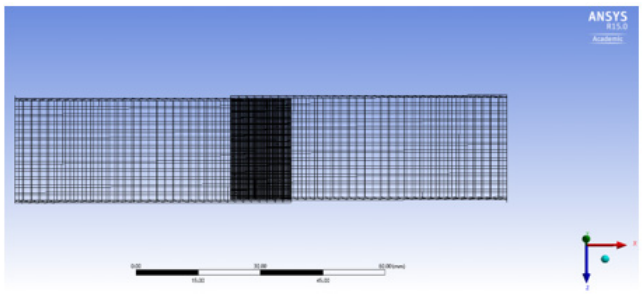

Figure 7. A representative modeling of the *A* specimen for the finite element analysis; the A_r, *B*, and B_r specimens were also investigated in actual size.

3.2. Stress-strain curves for SLJ specimens

Fig. 6 shows the locations of strain gauges attached to the front and backside adherends of the SLJ specimens. The numbers of strain gauges attached to the backside adherends are shown in parentheses. Strain gauges were attached symmetrically to an SLJ specimen (see Fig. 4). For the FEA modeling, the SLJ specimens were sketched in three-dimensional shapes and assembled using SolidWorks 2012. ANSYS 15.0 was used for all FEA modeling to measure the mechanical properties, including the strains and reaction forces on the adherends and peel and shear stresses in the adhesive[20]. The adherend and adhesive were treated as an isotropically elastic in the FEA modeling. The elastic moduli of the adherend and adhesive were 71 [20] and 2.38 GPa (see Table 2), respectively. Poison's ratios of the adherend and adhesive were 0.33 [20] and 0.37 (see Table 2), respectively. The meshes of the adherend and adhesive were 2 and 0.2 mm,

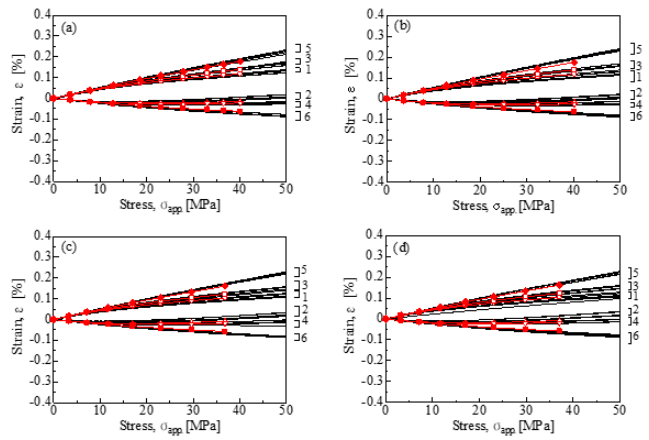

Figure 8. Stress-strain curves for the SLJ specimens, where (a), (b), (c), and (d) present the results for the *A*, A_r, *B*, and B_r specimens, respectively. Black lines were recorded for strain gauges attached to the front and backside of the adherends. Data sets numbered 1 to 6 were recorded using strain gauges (see Fig. 6). Red dots are the results obtained by finite element analysis methods.

respectively. Fig. 7 shows the geometry of the *A* specimen, where FEA modeling was used for comparison with the experimental values. The A_r, *B,* and B_r specimens were also modeled in full scale.

Fig. 8(a), (b), (c), and (d) show the stress-strain curves for the *A*, A_r, *B*, and B_r specimens, respectively. The black lines in Fig. 8(a)-(d) represent data obtained by experimental methods. The numbers from 1 to 6 in Fig. 8(a)-(d) represent the number of strain gauges attached to the front and backside adherends, respectively. The experimental data of the strain gauges attached symmetrically to adherends are plotted together in Fig. 8. The red dots of ○, △, □, ▽, ◆, and ■ in Fig. 8(a)-(d) indicate the values obtained from FEA methods, corresponding to strain-gauge locations 1, 2, 3, 4, 5, and 6. The strain values measured by strain gauges 1, 3, and 5 and those determined by FEA methods increased with increasing stress. These results suggest that the adherend was in tension as the load was applied. Even though the values for the stress and strain were measured at almost 40 MPa, the stress-strain curves obtained experimentally were in good agreement with those obtained through FEA.

3.3. Average shear strength

The average shear strength ($\bar{\tau}_{max}$) for SLJ specimens can be written as

$$\tau_{max} = P_{max} / A, \quad (1)$$

where P_{max} and A are the applied maximum load and the area of the bonded part, respectively. Fig. 9 shows the τ_{max} results for the SLJ specimens. Error bars indicate the standard deviation (S.D.). The values of τ_{max} and C.V. are summarized in Table 3. The value of τ_{max} for the *Ar* specimen was greater than that of the *A* specimen. However, no substantial differences were observed in the values of τ_{max} between *B* and B_r specimens. These results confirm that specimen *A* exhibited the smallest τ_{max} value among the four different specimens. The effect of adhesive thickness on shear strength for SLJ specimens bonded with epoxy adhesive has been reported to be inconsequential in the thickness range from 0.03 to 0.7 mm [13]. We therefore reasonably assumed that the thin adhesive layer used in the present study had little effect on the shear strength of the SLJ specimens.

Table 3. Summary of average shear strength and coefficient of variation (C.V.) for SLJ specimens

	Specimens			
	A	*Ar*	*B*	*Br*
Average shear strength, τ_{max} [MPa]	19.2	22.0	20.1	20.6
C.V. [%]	4.5	5.0	2.9	5.4

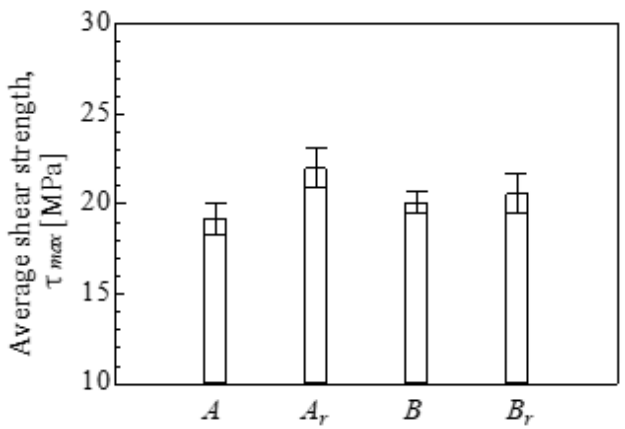

Figure 9. Average shear strength for the SLJ specimens. Error bars indicate the standard deviation (S.D.).

FEA methods were used to measure the adhesive stress distributions (peel and shear stresses) in the bonded part of the SLJ specimens. Fig. 10(a) shows a schematic of the measurement locations for the adhesive stress distributions, where x and c represent the measured distance from the center and the half-length of the bonded part, respectively. Fig. 10(b) and (c) show the results of the adhesive stress distributions for the *A*, A_r, *B*, and B_r specimens. The applied stress (σ_{app}) was measured by dividing the load by cross-sectional area of an adherend. Lines with and without dots represent peel and shear stresses, respectively. The positions corresponding to the center, 11 mm from the center line, and the surface of the bonded part are denoted as $z = 0$, $z = 11$, and $z = 13$, respectively. In all cases, we confirmed that the peel and shear stresses decreased as the measurement locations were shifted from the center ($z = 0$) to the surface ($z = 13$) of the bonded part. In addition, the values of the peel and shear stresses for all specimens approached zero as the measurement locations were moved to the central location (x/c = 0.5) in the bonded part, as shown in Fig. 10(b) and (c). Several studies were reported about the peel and shear stress trends using the SLJ specimens [21-25]. No substantial differences were observed in the adhesive stress distributions between *B* and B_r specimens, as shown in Fig. 10(c). Based on the results of the FEA methods, it can be considered that similar values of τ_{max} for *B* and B_r specimens were attributed to similar adhesive stresses. However, the *A* specimen showed high values of peel stress at locations $z = 0$ and $z = 11$, as shown in Fig. 10(b). In addition, the values of shear stress for specimen *A* remained the same until 0.1 of the x axis, as shown in Fig. 10(b). These trends indicate that stress was highly concentrated at the edge of the bonded part on specimen *A* as compared with that at the edge of the bonded parts on the other specimens. Thus, the smallest value of τ_{max} for specimen *A* (see Table 3) was caused by high stress concentrations (peel and shear stresses) at the edge of the bonded part.

3.4. Fracture surface observations

A microscope (VH-ZST swing-head zoom lens, VHX-5000 digital microscope, Keyence Corp., Japan) was used for the microscopic analysis of the fracture surfaces. Fig. 11(a), (c), (d), and (e) show the fracture surfaces of the bonded part for specimens *A*, A_r, *B*, and *Br*, respectively. A pair of fractured surfaces of an SLJ specimen was placed in the direction of the applied load, as shown in Fig. 11(a), (c), (d), and (e). Fig. 11(b) and (f) are enlarged views of the specimens shown in (a) and (e), respectively. Small particles of adhesives were observed on the fracture surfaces of the aluminum alloy, as shown in Fig. 11(b)

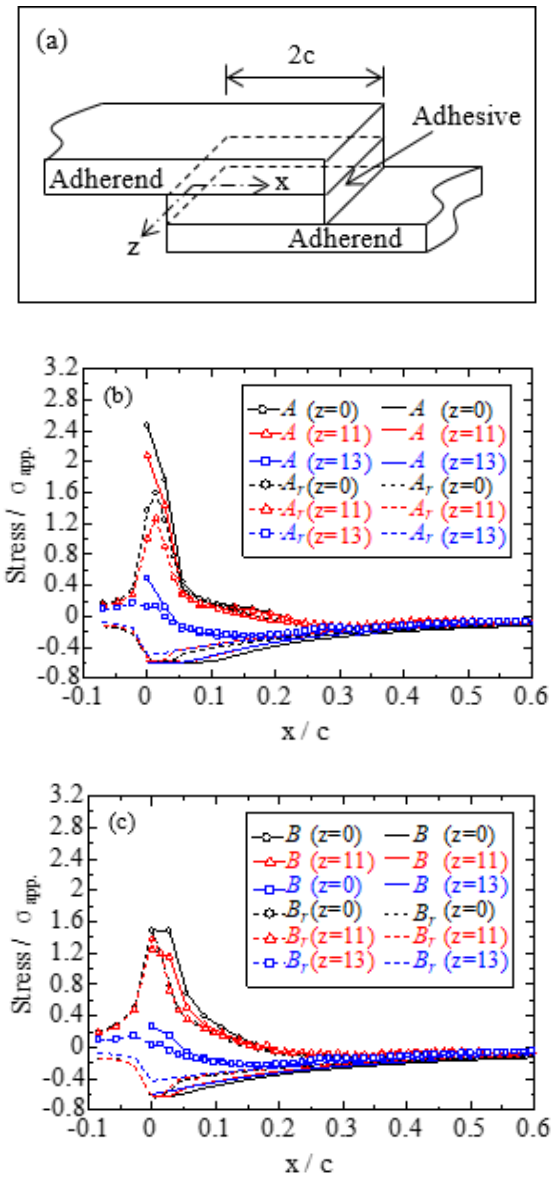

Figure 10. Adhesive stress distributions for SLJ specimens. Lines with and without dots indicate peel and shear stresses, respectively; z = 0, z = 11, and z = 13 indicate the locations corresponding to the center, a point 11 mm from the center, and the surface in the bonded part of the SLJ specimens, respectively, and x and c are the measurement locations corresponding to the center and to the half-length of the bonded part.

and (f). Adhesives of round fillets for the *Ar* and *Br* specimens remained on the surfaces of the aluminum alloy, as shown in Fig. 11(c) and (e). These results indicate that crack propagation in the *Ar* and *Br* specimens occurred between the end faces of the adherend and the

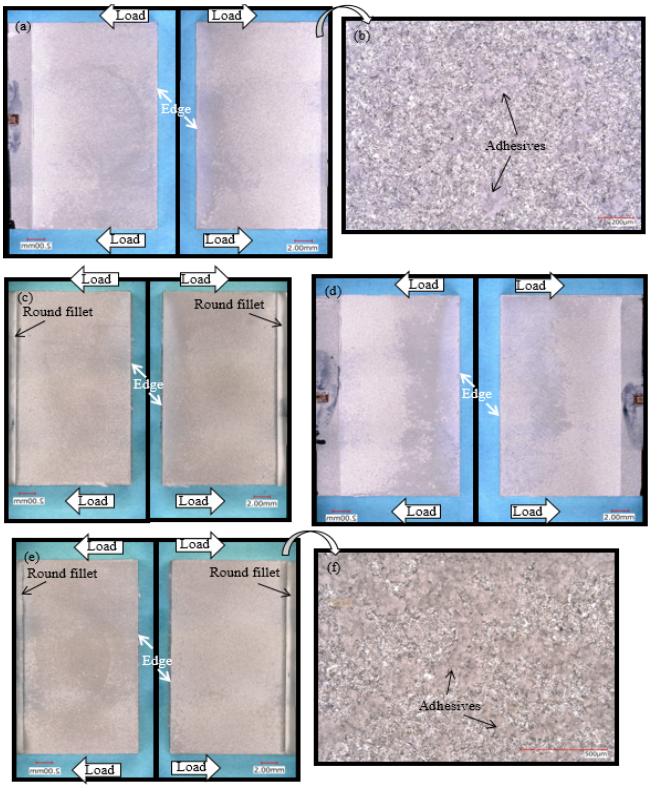

Figure 11. Fracture surfaces of (a), (c), (d), and (e) are taken from *A*, A_r, *B*, and B_r specimens, respectively. The fracture surfaces of (b) and (f) are enlarged views of (a) and (e), respectively.

partial round fillets. One of the reasons for these failures was poor adhesion along the end face. However, other authors have noted that such joints do not substantially differ in strength[2].

4. Conclusion

SLJ specimens with and without round fillets were subjected to tensile tests to measure the average shear strength in different lengths of adherend. Tensile tests for the bulk adhesive specimen were conducted to measure the mechanical properties such as the Young's modulus and the Poisson's ratio, and the obtained experimental data were used for FEA. The results confirm that the stress–strain curves for SLJ specimens recorded experimentally and those modeled with FEA methods showed good agreement with each other. The adhesive stress distributions obtained by FEA methods well supported the explanation of the difference in the average shear strength of the SLJ specimens.

Acknowledgements

This work was supported by the NIMS Joint Research Hub Program. We would also like to thank Professor Takashi Kobayashi, Numazu College, who provided insight and expertise that greatly assisted the research.

Conflict of interest: The authors declare that we have no conflict of interest.

References

1. D.A. Bigwood and A.D. Crocombe, *International Journal of Adhesion and Adhesives*, **9**, 229-242 (1989).
2. J.A. Harris and R.D. Adams, *International Journal of Adhesion and Adhesives*, **4**, 65-78 (1984).
3. M. Papini, G. Fernlund, and J.K. Spelt, *International Journal of Adhesion and Adhesives*, **14**, 5-13 (1994).
4. F.L. Matthews, P.F. Kilty, and E.W. Godwin, *Composite*, 29-37 (1982).
5. Paul A Cooper and James Wayne Sawyer, *NASA Technical Paper*, 1-59 (1979).
6. Chihdar Yang and Su-Seng Pang, *Composite Engineering*, **3**, 1051-1063 (1993).
7. R.D.S.G. Campilho, M.F.S.F. de Moura, and J.J.M.S. Domingues, *Composite Science and Technology*, **65**, 1948-1958 (2005).
8. M. Quaresimin and M. Ricotta, *Composite Science and Technology*, **66**, 647-656 (2006).
9. R.D.S.G. Campilho, M.D. Banea, J.A.B.P. Neto, and L.F.M. da Silva, *International Journal of Adhesion and Adhesives*, **44**, 48-56 (2013).
10. M. Quaresimin and M. Ricotta, *Composite Science and Technology*, **66**, 176-187 (2006).
11. R.D.S.G. Campilho, M.D. Banea, J.A.B.P. Neto, and L.F.M. da Silva, *International Journal of Adhesion & Adhesives*, **44**, 48-56 (2013).
12. Lucas F.M. da Silva, T.N.S.S. Rodrigues, M.A.V. Figueiredo, M.F.S.F. de Moura, and J.A.G. Chousal, *The Journal of Adhesion*, **82**, 1091-1115 (2006).
13. Ramazan Kahraman, Mehmet Sunar, and Bekir Yilbas, *Journal of Material Processing Technology*, **205**, 183-189 (2008).
14. Murat Demir Aydin, Adnan Ozel, and Semsettin Temiz, *Journal of Adhesion Science and Technology*, **19**, 705-718 (2005).
15. M.Y. Tsai and J. Morton, *Mechanics of Materials*, **20**, 183-194 (1995).
16. *Technical data sheet*, 3MTM Scotch-WeldTM Epoxy adhesives DP460 Off-White and DO460NS (2019).
17. H.-B. KIM, K. NAITO, and H. OGUMA, *Fatigue & Fracture of Engineering Materials & Structures*, **40**, 1795-1808 (2017).
18. "Rubber, vulcanized or thermoplastics-determination of tensile stress-strain properties," JIS K 6251 (2010).
19. "Adhesives for general works," JIS S 6040 (1995).
20. ANSYS, Release 15.0, ANSYS, Inc. (2013).
21. Dick J. Chang and R. Muki, *International Journal of Solids and Structures*, **10**, 503-517 (1974).
22. W. James Penton and Jack R. Vinson, *The Journal of Adhesion*, **7**, 175-193 (1975).
23. Gang Li, Pearl Lee-Sullivan, *International Journal of Adhesion & Adhesives*, **21**, 211-220 (2001).
24. J.N. Boss, V.K. Ganesh, and C.T. Lim, *Composite Structures*, **62**, 113-121 (2003).
25. Chihdar Yang, Hai Huang, John S. Tomblin, and Wenjun Sun, *Journal of Composites Materials*, **38**, 293-309 (2004).